

**Adhesion-stabilizing long-distance transport of cells on tissue surface**Katsuyoshi Matsushita *Department of Biological Sciences, Osaka University, Toyonaka, Osaka, Japan* (Received 3 November 2019; revised manuscript received 8 March 2020; accepted 12 May 2020; published 27 May 2020)

The stable transport of migrating eukaryotic cells is essential in organ development and repair processes. However, the mechanism that preserves transport stability over long distances in organs is not fully understood. As the driving mechanism of cell migration, the expressions of heterophilic cell-cell adhesion between moving cells and scaffolding tissue have been observed in such transport. In this paper, we theoretically investigate this heterophilic adhesion, which is persistently polarized in the migrating cell, as a possible transport stabilization mechanism. The adhesion was examined on the basis of the cellular Potts model, and our results confirm the stabilization of the transport to be an effect of the persistence.

DOI: [10.1103/PhysRevE.101.052410](https://doi.org/10.1103/PhysRevE.101.052410)**I. INTRODUCTION**

The stable transport of cells during their migration is important for a variety of biological processes in eukaryotes, including organogenesis and organ repair [1–4]. This process involves long-distance transport over distances far beyond the cell size ( $\simeq 10 \mu\text{m}$ ) and comparable to the organ scale ( $\simeq \text{mm}$ ) even in fluctuating environments. Long-distance transport is commonly observed in various species including mice [5], zebrafish [6], flies [7], and ascidians [8], and indicates the stabilization mechanism commonly underlying these organisms. Long-distance transport is considered to be supported by various chemical and mechanical signals [9]. The clarification of the stabilization mechanism based on these factors is an open problem in understanding biological processes from a physical perspective. Because real systems are complex, theoretical studies of simplified models focusing on each individual factor are performed to promote understanding.

Experimental and theoretical examinations thus far have focused on the chemotaxis of cells sensing the gradient of the attractant [10–12]. In the present theoretical study, we focus on another possibility, cell adhesion, which is a significant chemical factor in guiding cell action. Cell adhesion molecules are well known to be expressed during the transport of migrating cells including neurogenesis [13] and vasculogenesis [14]. Using these molecules, cells interact with the surrounding scaffolds and migrate in the proper direction. For example, in the development of mice, neurons are transported on their surrounding scaffolds consisting of radial glia, astrocytes, and blood vessels [5,15]. In this case, the cell adhesion through heterophilic adhesion molecules between neurons and scaffolds [16] is a powerful candidate factor for stable transport when the transport distance is of the order of 2–3 mm and is several hundred times larger than the typical size of cells. To consider it as the underlying stabilization mechanism of the transport, we model the cell adhesion between the migrating cells and scaffolds.

For this, we attempt to get hints from a previous work on the role of cell adhesion as the driving force of collective

cell migration with persistence [17]. In the previous theoretical model, homophilic cell-cell adhesion is supposed to be polarized, and its polarized direction follows the direction of cell migration. This polarization is observed in *Dictyostelium discoideum* [18] as an accumulation of Ddcad1, which is a homophilic adhesion protein, in the leading edge of cells and is expected to stabilize the collective migration in their aggregation. In the simulation, the cells interact with each other through homophilic polarized cell-cell adhesion and mutually guide their motions in the same direction. They finally stabilize in unidirectional collective migration with persistence. A similar mechanism may also be effective in stabilizing the long-distance transport of migrating cells on scaffolding tissues.

Here, the migrating cells on scaffolding tissue are called transported cells and the cells of the scaffolding epithelial tissue are called scaffolding cells, as shown in Fig. 1(a). We also simply call these “type,” following convention [19,20]. We assume a heterophilic cell-cell adhesion, which induces the interaction between the transported and scaffolding cells. Namely, the adhesion does not work between the same types of cells and only works between transported and scaffolding cells. Following previous work [17], we consider a polarization in the adhesion molecule density on the membrane of transported cells and assume isotropic density on the membrane of scaffolding cells. With these settings, we attempt to theoretically demonstrate the unidirectional transport of cells as shown in Fig. 1(b) and to confirm the long-distance persistence during cell motion. Specifically, we examine whether the transported cells avoid the continuous repetition of back and forth through collisions.

In the present paper, we simulate the one-dimensional transport of cells on a scaffolding tissue to examine persistently polarized heterophilic cell adhesion for the stabilization of long-distance transport. We consider the transported cells which autonomously exhibit only a random walk without interacting scaffolds through heterophilic adhesion. Such cell transports have been investigated theoretically with the focus on the movement mechanism of a cell based on its adhesion

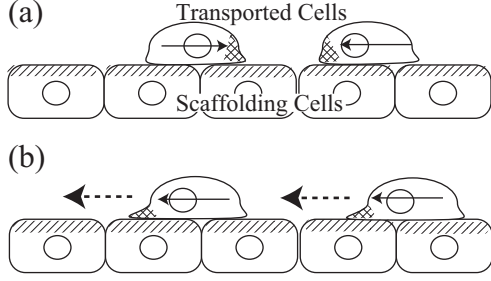


FIG. 1. (a) Schematic of cell transport on a tissue because of cell-cell adhesion. The arrows in cells represents the polarized direction of cell adhesion. The cross- and diagonal-hatched regions represent the high-density region of heterophilic adhesion molecules on the transported and scaffolding cells. (b) The unidirectional motion of transported cells. Arrows with dashed lines represent the migrating directions of cells.

[21,22]. Here, we now focus on the alignment in the cell movements of the transported cells. We showed that, during strong heterophilic adhesion and the long relaxation time of its polarity, the migration of cells is unidirectional even with only their repulsive interaction, and this direction is persistently maintained over long distances.

## II. MODEL AND METHOD

For our work, the two-dimensional cellular Potts model is considered [19,23–26]. In this model, the Potts states  $\{m(\mathbf{r})\}$  on the square lattice express cell configurations. Here,  $m(\mathbf{r})$  is a Potts state at the site  $\mathbf{r}$ .  $m(\mathbf{r})$  takes a number in the range from 0 to  $N$ , where  $N$  is the number of cells.  $m(\mathbf{r}) = 0$  indicates that the site  $\mathbf{r}$  is empty. Otherwise,  $m(\mathbf{r})$  represents the index of cells occupying the site  $\mathbf{r}$ . For simplicity, we consider a fixed  $N$  value.

In this model, the dynamics of the cells are reproduced by a Monte Carlo simulation, in which the Hamiltonian  $\mathcal{H}$  is formulated by the five terms

$$\mathcal{H} = \mathcal{H}_S + \mathcal{H}_T + \mathcal{H}_{ij} + \mathcal{H}_{ha} + \mathcal{H}_a. \quad (1)$$

The first and second terms on the right-hand side of Eq. (1) represent the surface energy of the scaffolding (S) and transported (T) cells, respectively. Both terms commonly take the form

$$\mathcal{H}_\alpha = \sum_{\mathbf{r}\mathbf{r}'} \eta_{m(\mathbf{r})m(\mathbf{r}')} (\Gamma_\alpha \delta_{\alpha\tau(m(\mathbf{r}))} \delta_{\alpha\tau(m(\mathbf{r}'))} + \Gamma_0 (\delta_{\alpha\tau(m(\mathbf{r}))} \eta_{0m(\mathbf{r}')} + \delta_{0m(\mathbf{r})} \delta_{\alpha\tau(m(\mathbf{r}'))})), \quad (2)$$

where  $\alpha$  denotes the type and takes either S or T. The  $m$ th cell  $\tau(m)$  takes the type S when it is a scaffolding cell and T when it is a transported cell.  $\delta_{\alpha\beta}$  denotes Kronecker's delta and  $\eta_{\alpha\beta}$  denotes  $1 - \delta_{\alpha\beta}$ .  $\Gamma_\alpha$  and  $\Gamma_0$  represent the surface tension between cells with the type  $\alpha$  and cell-empty space interfaces, respectively. For scaffolding cells, we take  $\Gamma_S < 2\Gamma_0$  to represent the adhesive interaction [24]. This condition corresponds to the assumption that the adhesion represents an adherence junction. In contrast, for transported cells, we take  $\Gamma_T > 2\Gamma_0$  to impose their repulsive interaction. The summation of the pair  $\mathbf{r}$  and  $\mathbf{r}'$  is taken over all the nearest-

and second-nearest-neighbor sites. Hereafter, the summation of all the pairs of  $\mathbf{r}$  and  $\mathbf{r}'$  are taken in the same manner.

We assume that the scaffolding cells are epithelial. The third term in Eq. (1) represents the tight junction [27,28] which inhibits their rearrangement. This term takes the form

$$\mathcal{H}_{ij} = -\Gamma_{ij} \sum_{\mathbf{r}\mathbf{r}'} \zeta_{m(\mathbf{r})m(\mathbf{r}')} \eta_{m(\mathbf{r})m(\mathbf{r}')}. \quad (3)$$

Here,  $\zeta_{mm'}$  takes the value of unity when the  $m$ th and  $m'$ th cells are neighboring scaffolding cells in the initial configuration; otherwise, it takes the value of 0. We take positive  $\Gamma_{ij}$  to inhibit the rearrangement of scaffolding cells from the initial configuration.

The fourth term represents the heterophilic adhesion between the scaffolding and transported cells. The term is formulated by

$$\mathcal{H}_{ha} = \sum_{\mathbf{r}\mathbf{r}'} [\delta_{\tau(m(\mathbf{r}))T} \delta_{\tau(m(\mathbf{r}'))S} (\Gamma_0 - \Gamma_{ha} \mathbf{e}_{m(\mathbf{r})}(\mathbf{r}) \cdot \mathbf{p}_{m(\mathbf{r}))} + \delta_{\tau(m(\mathbf{r}))S} \delta_{\tau(m(\mathbf{r}'))T} (\Gamma_0 - \Gamma_{ha} \mathbf{e}_{m(\mathbf{r}')}(r') \cdot \mathbf{p}_{m(\mathbf{r}'))})]. \quad (4)$$

Here,  $\mathbf{p}_m$  represents a unit polarity vector for the cell adhesion for the  $m$ th cell [17,29–31]. In the direction of  $\mathbf{p}_m$ , the surface tension is reduced by  $\Gamma_{ha}$  owing to the effect of the adhesion. This term promotes the leading-edge extension of transported cells and drives their motion. The microscopic origin is assumed to be intercellular transport [32] or the clutch mechanism [33]. As another microscopic origin, the slip-bond mechanism may also be possible [21,34,35]. For stabilizing cellular contacts due to this adhesion, we impose  $\Gamma_0 - (\Gamma_0 - \Gamma_{ha})/2 > 0$ .  $\mathbf{p}_m$  is a variable and obeys the equation of motion [31,36],

$$\frac{d\mathbf{p}_m}{dt} = \frac{1}{\tau a} [\hat{I} - (\mathbf{p}_m^\dagger \otimes \mathbf{p}_m)] \cdot \frac{d\mathbf{R}_m}{dt}, \quad (5)$$

where  $t$  is the time,  $a$  is the lattice constant, and  $\tau$  is a nondimensional parameter proportional to the relaxation time of  $\mathbf{p}_m$ . The tensor  $\hat{I}$  is the unit matrix, and  $\otimes$  represents the tensor product.  $\mathbf{R}_m$  is a parameter of the adhesion molecule density, which is quasistatically equal to the center coordinate of the  $m$ th cell,  $\sum_{\mathbf{r}} \mathbf{r} \delta_{m\mathbf{r}} / \sum_{\mathbf{r}} \delta_{m\mathbf{r}}$  [31].  $\mathbf{p}_m$  is analogous to the chemical compass for the chemotaxis [37] and is recognized as a compass for the cell-scaffold adhesion.  $\mathbf{p}_m$  follows the cell motion  $d\mathbf{R}_m/dt$ , whereas the chemical compass follows the chemical gradient.

According to this equation, the polarized adhesion is assumed to be stabilized by an intracellular transport of adhesion molecules in the cell migrating direction [32]. In contrast, the dynamics of adhesion molecule density, which is expressed as an expansion of  $\rho(\mathbf{r}) = \rho_0 + \rho_1 \mathbf{e}_{m(\mathbf{r})} \cdot \mathbf{p}_m + \dots$  [31], reflects the relaxation of Hamiltonian  $\mathcal{H}$ . The relaxation destabilizes the polarity and enhances the higher-order term in the above expansion if the relaxation is not negligible in comparison with the stabilization of the polarity due to intracellular transport. Therefore, this equation is based on the assumption that the relaxation is negligible and is justified only for this case. This has been commonly assumed in theoretical work for the cell polarity dynamics in the literature [38,39] and has explained cell migration well. In the present paper, as a simple

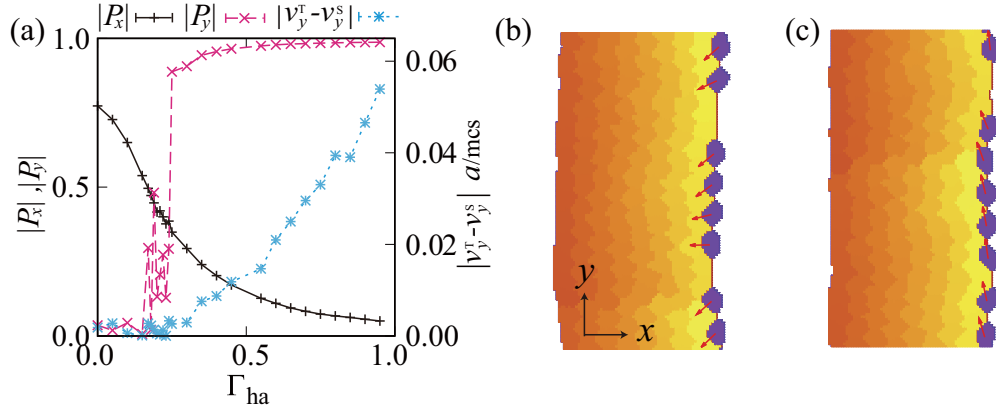


FIG. 2. (a)  $|P_x|$  (+),  $|P_y|$  ( $\times$ ), and  $|v_y - v_y^0|$  (\*) as functions of  $\Gamma_{ha}$ . Snapshots of the simulation for (b)  $\Gamma_{ha} = 0.1$  and (c)  $\Gamma_{ha} = 0.5$ . Yellow or orangelike (light) colored regions represent scaffolding cells and violet (dark) colored regions represent transported cells. Differences in color represent different cells. White regions represent empty space. Red arrows represent the polarities of cell adhesion. The directions of the coordination axes are given in (b).

case study, we employ this assumption and limit the focus of this work only to this case.

The fifth term represents the area constraint of cells to a constant value  $V$ . The term is given by

$$\mathcal{H}_a = \kappa \sum_m \left( 1 - \frac{\sum_r \delta_{mm(r)}}{V} \right)^2. \quad (6)$$

It may be noted that these five terms do not exert migration force on cells when they are isolated, in contrast to previous works with spontaneous migrating force [36,39,40]. When the scaffolding and transported cells make contact, migration force is exerted on the transported cells as an effect of the heterophilic polarized cell adhesion in Eq. (4). In addition, when polarized cell adhesion is absent, the migration force disappears and a random walk emerges.

To simulate the dynamics of cells, we consider the following Monte Carlo procedure: A Monte Carlo step conventionally consists of  $16L^2$  copy trials [19], where  $L$  is the system size. In a single copy trial, a site  $\mathbf{r}$  is randomly chosen first, after which a neighboring site  $\mathbf{r}'$  is randomly chosen in the nearest and next-nearest sites. The copy of the Potts state from  $\mathbf{r}'$  to  $\mathbf{r}$  is accepted with the Metropolis probability  $\min\{1, \exp[-\beta(\mathcal{H}_c - \mathcal{H})]\}$ , where  $\mathcal{H}_c$  is the value of  $\mathcal{H}$  when  $m(\mathbf{r}')$  is copied to  $m(\mathbf{r})$ . Otherwise, the copy is rejected. This procedure is repeated in the simulation and generates the cell configuration. The time series of the cell configuration expresses the transported cell migration. For each Monte Carlo step,  $\mathbf{p}_m$  and  $\mathbf{R}_m$  are fixed in the assumption that they are slow variables [31].  $\mathbf{p}_m$  is once updated by solving Eq. (5) with  $\mathbf{R}_m$  between every two consecutive Monte Carlo steps. In the update of  $\mathbf{R}_m$ , we use  $\mathbf{R}_m = \sum_r \mathbf{r} \delta_{mm(r)} / \sum_r \delta_{mm(r)}$ .

Consider a square lattice system with  $L = 128$  with a periodic boundary condition. We consider 128 scaffolding and eight transported cells. In the initial state, the scaffolding cells form a band configuration [see Figs. 2(b) and 2(c)]. The scaffolding-cell configuration has a triangular lattice consisting of 8 and 16 cell arrays in the  $x$  and  $y$  direction, respectively. Here, the directions are defined in Fig. 2(b). A band of scaffold is connected to itself at the boundary in the  $y$  direction. This

initial state is a stable state of the Hamiltonian and is chosen to shorten the relaxation time to the stable state. The eight transported cells are initially distributed at random positions on the surface on the right-hand side of the band in Fig. 2(b). In this initial state, the polarities of the transported cells are randomly aligned.

We determine the adhesion parameters by imposing the following conditions. The first condition is  $\Gamma_{ij} > \Gamma_{ha}$  to realize a stronger tight junction than the heterophilic adhesion to avoid the destabilization of the junction owing to the adhesion. The second condition is  $\Gamma_S > \Gamma_{ij}$  to realize a positive tension of scaffold cells, which is necessary for the stability of the scaffold cells. The third condition is  $(\Gamma_0 - \Gamma_{ha}) - (\Gamma_S - \Gamma_{ij})/2 > 0$  to make the scaffolding tissue be stable against the interaction effect of the scaffold and the transported cells. Furthermore, to maintain the stability of the scaffold and the suspension of transported cells, we impose  $\Gamma_0 - \Gamma_S/2 > 0$ ,  $\Gamma_0 - \Gamma_T/2 < 0$ , and  $\Gamma_0 - (\Gamma_0 - \Gamma_{ha})/2 > 0$ . To satisfy all of these conditions, we employ the surface tension values as  $\Gamma_0 = 6.0$ ,  $\Gamma_S = 4.0$ ,  $\Gamma_T = 13.0$ , and  $\Gamma_{ij} = 2.0$ .

The heterophilic adhesion  $\Gamma_{ha}$  is known to be in the order of 1 pN/nm [21]. The values of these tension parameters correspond to the order of several 10 pN/nm. For the adherence junction  $\Gamma_S$ , this value corresponds to the previously estimated value 50 pN/nm in the order [41]. In addition, we adopt the parameters  $V = 64$ ,  $\kappa = 0.3V^2$ , and  $\beta = 0.5$  from previous works [40] because they can move easily.

### III. RESULT

We now confirm the unidirectional transportation of cells on the scaffolding tissue through the simulation of this model. We consider a large relaxation time value for the adhesion polarity  $\tau$ ,  $\tau = 5.0$ , because, based on the previous study on collective migration [40], the unidirectional transportation is expected to require a long relaxation time for the adhesion polarity. The unidirectional transport of cells is expected to be reflected by the adhesion polarity order of the transported cells. Using this expectation, we examine the unidirectional transport by calculating the order parameter of the adhesion

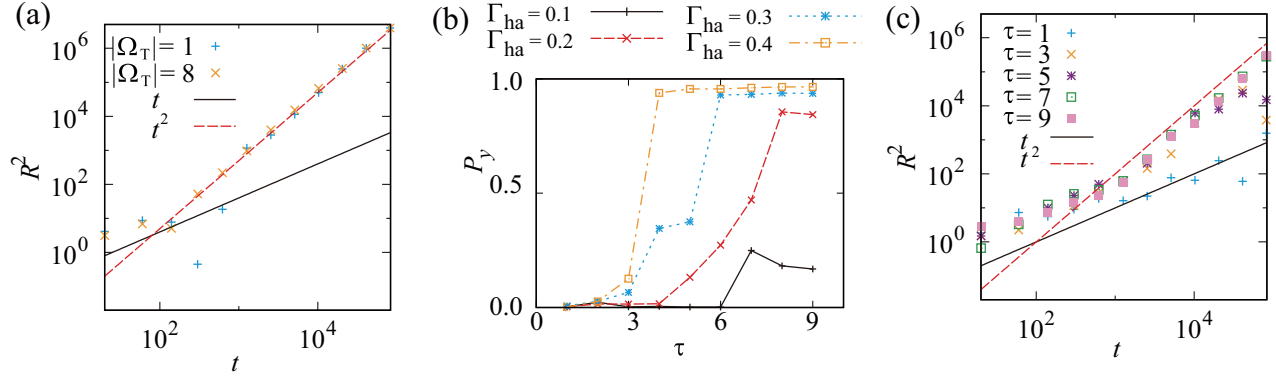


FIG. 3. (a) The mean-square distance of a cell motion  $R^2$  for  $N = 1$  (+) and  $N = 8$  (×) with  $\Gamma_{ha} = 0.5$  and  $\tau = 5.0$ . The solid and dashed lines represent  $t$  and  $t^2$ , respectively. (b)  $|P_y|$  as a function of relaxation time of  $\mathbf{p}_m$ ,  $\tau$  for  $\Gamma_{ha} = 0.1$  (solid line),  $\Gamma_{ha} = 0.2$  (dashed line),  $\Gamma_{ha} = 0.3$  (dotted line),  $\Gamma_{ha} = 0.4$  (dashed-dotted line). (c) The mean-square distance of a cell motion  $R^2$  for  $\tau = 1$  (+),  $\tau = 3$  (×),  $\tau = 5$  (\*),  $\tau = 7$  (□), and  $\tau = 9$  (■) with  $\Gamma_{ha} = 0.2$ . The solid and dashed lines represent  $t$  and  $t^2$ , respectively.

polarity,

$$\mathbf{P} = \frac{1}{T} \int_{T_0}^T dt \frac{1}{|\Omega_T|} \sum_{m \in \Omega_T} \mathbf{p}_m, \quad (7)$$

where  $\Omega_T$  represents the set of indices for transported cells, and its cardinal represents the number of transported cells.  $T_0$  is the number of Monte Carlo steps to be used for relaxation to the steady state.  $T$  is the number of Monte Carlo steps for the time average. We employ  $T_0 = 2 \times 10^4$  and  $T = 5 \times 10^5$ . In this simulation, because the scaffolding cells form a band-configured tissue in the  $y$  direction, the transport of cells also occurs in the  $y$  direction. Therefore, we focus on the  $y$  component of  $\mathbf{P}$ ,  $P_y$ .

We plot the absolute values of components of  $\mathbf{P}$ , namely,  $|P_x|$  and  $|P_y|$ , as functions of  $\Gamma_{ha}$  in Fig. 2(a). For low values of  $\Gamma_{ha}$ ,  $|P_x|$  is much larger than  $|P_y|$ . In contrast, for large values of  $\Gamma_{ha}$ ,  $|P_y|$  is much larger than  $|P_x|$ . This behavior can be confirmed in the snapshots of steady states for  $\Gamma_{ha} = 0.1$  and  $0.5$ , shown in Figs. 2(a) and 2(b), respectively. From these results, it can be seen that the cells avoid repetition of the back and forth movement and realize unidirectional transport with the polarity order for large values of  $\Gamma_{ha}$ .

To directly confirm the unidirectional transport of cells, we calculate the  $y$  component of the time average velocity of transported cells  $v_y^T$ . Note that the shapes of the scaffolding cells fluctuate, and thus the scaffolding tissue moves diffusively. Therefore, the velocity should be measured relative to that of the scaffolding tissue,  $v_y^T - v_y^S$ , where  $v_y^S$  is the time average velocity of the mass center of the scaffolding tissue. The absolute value of the relative velocity  $|v_y^S - v_y^T|$  is also plotted as a function of  $\Gamma_{ha}$  in Fig. 2(a). When  $|P_x| > |P_y|$  with low  $\Gamma_{ha}$ , the average relative velocity is almost zero. When  $|P_x| < |P_y|$  with large  $\Gamma_{ha}$ , the velocity clearly has a finite value and increases at an accelerated pace with increasing  $\Gamma_{ha}$ . This directly indicates that strong heterophilic cell adhesion with the polarity realizes the unidirectional transport of cells on the scaffolding tissue.

Next, to examine the long-distance persistence of this transport, we calculate the mean-square displacement of the

transported cells with cell average  $R^2$ . We plot  $R^2$  as a function of  $t$  in Fig. 3(a);  $R^2$  behaves as  $t^2$  and indicates the persistent motion of transported cells. The behavior of  $t^2$  ranges in the order of  $10^6 a^2$ . Because the typical cell size is  $\sqrt{V} = 8a$ , the value of the range corresponds to the order of several hundred times the typical cell size. It implies that the heterophilic cell adhesion with polarity stabilizes the long-distance transport of cells.

Let us consider the possible origins of long-distance cell transport stability. One possible origin is the many-body effects due to the repulsive interaction of transported cells. To examine the effect of the interaction between transported cells, we also calculate  $R^2$  for  $|\Omega_T| = 1$  and plot it in the same figure. The  $R^2$  values for  $|\Omega_T| = 1$  show the same behavior as for  $|\Omega_T| = 8$  until a long  $t$  value is reached. Therefore, this comparison indicates that the interaction between transported cells is not necessary for persistence in transported cell motions; the interaction only affects the alignment directions of the cell motion [40].

The correlation between large  $|P_y|$  and unidirectional transport suggests another possible origin. The large values of  $|P_y|$  are expected to reflect not only  $\Gamma_{ha}$  but also the relaxation time of  $\mathbf{p}_m$ ,  $\tau$ . This is because  $|P_y|$  is stabilized by feedback control between  $\mathbf{R}_m$  and  $\mathbf{p}_m$  through Eq. (5) [17], where the feedback time is determined by  $\tau$ . To directly confirm the stabilization of  $P_y$  by the relaxation time  $\tau$ , we plotted  $|P_y|$  as a function of  $\tau$  for various  $\Gamma_{ha}$  in Fig. 3(b). For a small  $\Gamma_{ha}$ , below 0.3,  $P_y$  for a short  $\tau$  has low values. This indicates that the stability of  $P_y$  originates from a long  $\tau$ . Therefore, the long  $\tau$  stabilizes the unidirectional transportation in long distances through stabilizing  $P_y$ .

To directly confirm that long  $\tau$  stabilizes the unidirectional transport in long distances, we calculate  $R^2$  for various values of  $\tau$ . We choose  $\Gamma_{ha} = 0.2$  with marginal stable  $P_y$  to easily detect the effect of  $\tau$ . We plot the functions in Fig. 3(c).  $R^2$  changes from  $t$  to  $t^2$  on crossing from short to long  $\tau$  and indicates the extension of the distance with the stable transport. Thus, the relaxation time of the adhesion polarity is a possible origin for the stabilization of long-distance cell transport.

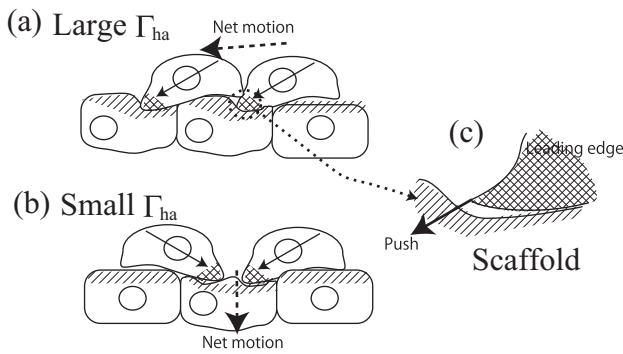


FIG. 4. The schematic view of cell behavior and push due to heterophilic adhesion for (a) large  $\Gamma_{ha}$  and for (b) small  $\Gamma_{ha}$ . (c) Magnified view of the leading edge. Solid and dashed arrows in (a) and (b) express the polarity and net motion, The solid arrow in (c) represents the push direction of the transported cell on the scaffold.

#### IV. SUMMARY AND REMARKS

In summary, we show that heterophilic cell adhesion can drive cell transportation. In this case, strong polarized adhesion and the persistence of polarity are necessary for the stable transport of cells over long distances. Note that while we only show this for a set of model parameters, which stabilizes the scaffold, the suspended state of transported cells, and the adhesion polarity due to intracellular transport, we naively expected similar results to be reproduced for parameters as long as the state is stable.

Our result predicts the elongation of a reachable distance for transported cells as the relaxation time of the polarity. The relaxation time corresponds to the persistent time of the cellular persistent random walk on adhesive substrates. The persistent random walk depends on the type [38] or developmental stage [42] of cells. Therefore, by using these cells with different types, it may be possible to check the elongation of the reachable distance of the cell transport.

Consider the mechanism of two states depending on  $\Gamma_{ha}$ , namely, large  $P_x$  for small  $\Gamma_{ha}$  and large  $P_y$  for large  $\Gamma_{ha}$ . These states are characterized by the net direction of the polarity  $\mathbf{P}$ . From Eq. (5), these directions of  $\mathbf{P}$  follow the direction of  $d\mathbf{R}_m/dt$  averaged over cells. Therefore, the directions of  $\mathbf{P}$

indicate that there exists a net collective cell motion in the  $x$  direction for small  $\Gamma_{ha}$  and in the  $y$  direction for large  $\Gamma_{ha}$ . Therefore, to explain these states, we consider the direction of the cell motion in these states.

For large  $\Gamma_{ha}$ , the rapid motion of transported cells generally tends to occur in the  $y$  direction, as shown in Fig. 4(a). This is because the transported cells are restricted by the scaffolding tissue and thereby mainly aligned their motion in the  $y$  direction. In this case, because rapid motion due to large  $\Gamma_{ha}$  exhibits an order state as a polarity memory effect [40,43–47], the net motion of the transported cells aligns  $\mathbf{P}$  in the  $y$  direction through Eq. (5).

In contrast, for small  $\Gamma_{ha}$ , the  $x$ -directional motion of transported cells implies that the restriction of scaffolding tissue is apparently ineffective in the determination of  $\mathbf{P}$ . This is due to  $\Gamma_{ha}$  being too small to induce order in cell motion in the  $y$  direction as shown in Fig. 4(b). The contribution of  $y$ -directional motion cancels itself and is averaged out at a low value in the determination of  $\mathbf{P}$ . Instead, the small net motion of the transported cells in the  $x$  direction, which is negligible for large  $\Gamma_{ha}$  in comparison with that in the  $y$  direction, emerges. This net motion is driven by pushing due to the energy gain of the heterophilic adhesion between the transported cells and the scaffolding tissue as shown in Fig. 4(c). This net motion finally aligns  $\mathbf{P}$  in the  $x$  direction through Eq. (5). As a result, the two states appear to be dependent on the values of  $\Gamma_{ha}$ .

Finally, we discuss the possibility of the realization of the state for small  $\Gamma_{ha}$ . In real systems, scaffolding tissues are supposed to be fixed in space. In this case, because of the absence of net motion in the  $x$  direction, the motion of the transported cells is expected to exhibit a simple random walk in the  $y$  direction. As a result, the transport of cells is expected to become diffusive for small cell adhesion.

#### ACKNOWLEDGMENTS

We would like to thank H. Kuwayama, H. Hashimura, S. Yabunaka, K. Horibe, N. Kamamoto, H. Sawamoto, M. Igarashi, N. Kaneko, and M. Sawada for insightful discussions. We also thank K. Fujimoto, M. Kikuchi, and H. Yoshino for their research resource support. This work is supported by JSPS KAKENHI (Grant No. 19K03770) and by AMED (Grant No. JP19gm1210007).

[1] C. M. Franz, G. E. Jones, and A. J. Ridley, *Dev. Cell* **2**, 153 (2002).  
 [2] R. Horwitz and D. Webb, *Curr. Biol.* **13**, R756 (2003).  
 [3] A. Aman and T. Piotrowski, *Dev. Biol.* **341**, 20 (2010).  
 [4] G. Reig, E. Pulgar, and M. L. Concha, *Development* **141**, 1999 (2014).  
 [5] C. Lois and A. Alvarez-Buylla, *Science* **264**, 1145 (1994).  
 [6] A. Ghysen and C. Dambly-Chaudière, *Curr. Opin. Neurobiol.* **14**, 67 (2004).  
 [7] M. K. Jaglarz and K. R. Howard, *Development* **121**, 3495 (1995).  
 [8] K. Kishi, T. A. Onuma, and H. Nishida, *Dev. Biol.* **395**, 299 (2014).

[9] A. J. Ridley, M. A. Schwartz, K. Burridge, R. A. Firtel, M. H. Ginsberg, G. Borisy, J. T. Parsons, and A. R. Horwitz, *Science* **302**, 1704 (2003).  
 [10] A. Bagorda and C. A. Parent, *J. Cell Sci.* **121**, 2621 (2008).  
 [11] T. Jin, *Curr. Opin. Cell Biol.* **25**, 532 (2013).  
 [12] P. A. Iglesias and P. N. Devreotes, *Curr. Opin. Cell Biol.* **20**, 35 (2008).  
 [13] P. Rakic, *Experientia* **46**, 882 (1990).  
 [14] W. Risau and I. Flamme, *Annu. Rev. Cell Dev. Biol.* **11**, 73 (1995).  
 [15] N. Kaneko, O. Marín, M. Koike, Y. Hirota, Y. Uchiyama, J. Y. Wu, Q. Lu, M. Tessier-Lavigne, A. Alvarez-Buylla, H. Okano, J. L. R. Rubenstein, and K. Sawamoto, *Neuron* **67**, 213 (2010).

- [16] S. Murase and A. F. Horwitz, *J. Neurosci.* **22**, 3568 (2002).
- [17] K. Matsushita, *Phys. Rev. E* **97**, 042413 (2018).
- [18] J. C. Coates and A. J. Harwood, *J. Cell Sci.* **114**, 4349 (2001).
- [19] F. Graner and J. A. Glazier, *Phys. Rev. Lett.* **69**, 2013 (1992).
- [20] A. F. M. Marée and P. Hogeweg, *Proc. Natl. Acad. Sci. USA* **98**, 3879 (2001).
- [21] J. H. Lopez, M. Das, and J. M. Schwarz, *Phys. Rev. E* **90**, 032707 (2014).
- [22] M. Leoni and P. Sens, *Phys. Rev. Lett.* **118**, 228101 (2017).
- [23] F. Graner, *J. Theor. Biol.* **164**, 455 (1993).
- [24] J. A. Glazier and F. Graner, *Phys. Rev. E* **47**, 2128 (1993).
- [25] M. Scianna and L. Preziosi, *Cellular Potts Models* (CRC Press, Oxfordshire, U.K., 2013).
- [26] T. Hirashima, E. G. Rens, and R. M. H. Merks, *Dev. Growth Differ.* **59**, 329 (2017).
- [27] E. E. Schneeberger and R. D. Lynch, *Cell Physiol.* **286**, C1213 (2004).
- [28] J. M. Anderson and C. V. Itallie, *Cold Spring Harb. Perspect. Biol.* **1**, a002584 (2009).
- [29] M. Zajac, G. L. Jones, and J. A. Glazier, *J. Theor. Biol.* **222**, 247 (2002).
- [30] R. M. A. Vroomans, P. Hogeweg, and K. H. W. J. ten Tusscher, *PLoS Comput. Biol.* **11**, e1004092 (2015).
- [31] K. Matsushita, *Phys. Rev. E* **95**, 032415 (2017).
- [32] T. Kawauchi, *J. Mol. Sci.* **13**, 4564 (2012).
- [33] G. Giannone, R.-M. Mège, and O. Thoumine, *Trends Cell Biol.* **19**, 475 (2009).
- [34] G. I. Bell, *Science* **200**, 618 (1978).
- [35] B. T. Marshall, M. Long, J. W. Piper, T. Yago, R. P. McEver, and C. Zhu, *Nature (London)* **423**, 190 (2003).
- [36] B. Szabó, G. J. Szollosi, B. Gonci, Z. Juranyi, D. Selmeczi, and T. Vicsek, *Phys. Rev. E* **74**, 061908 (2006).
- [37] H. R. Bourne and O. Weiner, *Nature (London)* **419**, 21 (2002).
- [38] A. Szabó, R. Ünneper, E. Méhes, W. O. Twal, W. S. Argraves, and Y. Cao, *Phys. Biol.* **7**, 046007 (2010).
- [39] A. J. Kabla, *J. R. Soc. Interface* **9**, 3268 (2012).
- [40] K. Matsushita, K. Horibe, N. Kamamoto, and K. Fujimoto, *J. Phys. Soc. Jpn.* **88**, 103801 (2019).
- [41] G. Charras and A. S. Yap, *Curr. Biol.* **28**, R445 (2018).
- [42] H. Takagi, M. J. Sato, T. Yanagida, and M. Ueda, *PLoS One* **3**, e2648 (2008).
- [43] C. A. Weber, T. Hanke, J. Deseigne, S. Léonard, O. Dauchot, E. Frey, and H. Chaté, *Phys. Rev. Lett.* **110**, 208001 (2013).
- [44] T. Hanke, C. A. Weber, and E. Frey, *Phys. Rev. E* **88**, 052309 (2013).
- [45] T. Hiraoka, T. Shimada, and N. Ito, *Phys. Rev. E* **94**, 062612 (2016).
- [46] T. Hiraoka, T. Shimada, and N. Ito, *J. Phys.: Conf. Series* **921**, 012006 (2017).
- [47] A. Martín-Gómez, D. Levis, A. Díaz-Guilera, and I. Pagonabarraga, *Soft Matter* **14**, 2610 (2018).